Kinetics of the Secretory Response in Bovine Chromaffin Cells Following Flash Photolysis of Caged Ca^{2+}

Christian Heinemann,* Robert H. Chow,* Erwin Neher,* and Robert S. Zucker[+]

*Department of Membrane Biophysics, Max-Planck-Institute for Biophysical Chemistry, D-37077 Göttingen, Germany; and [+]Department of Molecular and Cell Biology, University of California, Berkeley, California 94720 USA

ABSTRACT   The kinetics of the secretory response in bovine chromaffin cells following flash photolysis of caged Ca^{2+} were studied by capacitance (C_m) measurements with millisecond time resolution. After elevation of the internal Ca^{2+} concentration ([Ca^{2+}]$_i$), C_m rises rapidly with one or more exponentials. The time constant of the fastest component decreases for higher [Ca^{2+}]$_i$ (range 3–600 µM) over three orders of magnitude before it saturates at ~1 ms. The corresponding maximal rates of secretion can be as fast as 100,000 fF/s or 40,000 vesicles/s. There is a Ca^{2+}-dependent delay before C_m rises, which may reflect the kinetics of multiple Ca^{2+} ions binding to the secretory apparatus. The initial rise in C_m is described by models containing a sequence of two to four single Ca^{2+}-binding steps followed by a rate-limiting exocytosis step. The predicted Ca^{2+} dissociation constant (K_d) of a single Ca^{2+}-binding site is between 7 and 21 µM. At [Ca^{2+}]$_i$ > 30 µM clear indications of a fast endocytotic process complicate the analysis of the secretory response.

INTRODUCTION

Use of the electrochemical method amperometry to assay secretion (Kawagoe et al., 1993; Chow and von Rüden, 1994; Chow et al., 1992) showed that secretion in bovine chromaffin cells persists for tens of milliseconds after termination of a voltage-clamp depolarization. As the calcium current in these cells turns off in <1 ms at the end of the depolarization (Fenwick et al., 1982), the persistence of secretion occurs despite cessation of calcium entry. In contrast, secretion in synapses such as frog and crayfish neuromuscular junction (Katz and Miledi, 1965; Parnas et al., 1989) stops within a few milliseconds after a depolarizing stimulus ends. Persistence of secretion after Ca^{2+} injection has ceased could arise in chromaffin cells because the secretory machinery turns off slowly or because the calcium concentration at the secretory sites decays slowly back to basal levels. To evaluate the first possibility, we investigate here the kinetics of secretion in chromaffin cells.

In a previous study on bovine chromaffin cells, Neher and Zucker (1993) combined flash photolysis of caged Ca^{2+} compounds to achieve rapid elevation of Ca^{2+} and capacitance measurement at low time resolution to monitor secretion kinetics (Lindau and Neher, 1988). Electrical capacitance measurements give a readout of the cell membrane surface area, which increases upon exocytotic addition of vesicular membrane (Neher and Marty, 1982). Following a flash, there was a "fast" surge of capacitance increase (time constant 1–2 s), sometimes preceded by an "ultrafast" surge that was not resolved kinetically. After the initial surge, capacitance in-

creased much more slowly. The different phases of capacitance rise were interpreted to be due to the successive addition to the plasma membrane of vesicles residing in different functional pools, each having differing "readiness" for exocytosis.

In two other studies on pituitary melanotrophs (Thomas et al., 1993a, b), a similar pattern was observed. In these cases, the ultrafast response (termed "exocytotic burst") was studied at millisecond time resolution, and it was shown to start with extremely high rates (up to 4500 fF/s at high [Ca^{2+}]$_i$). There was also a delay between the time of the flash and the onset of the capacitance response. It was suggested that binding of three Ca^{2+} ions to regulatory sites contributes to this delay.

Here we show that flash photolysis of the caged Ca^{2+} compound (1-(2-nitro-4, 5-dimethoxyphenyl)-1,2-diaminoethane-N,N,N',N'-tetraacetic acid) (DM-nitrophen) (Kaplan and Ellis-Davis, 1988) in bovine chromaffin cells, as in melanotrophs, induces an ultrafast capacitance change, and, for smaller [Ca^{2+}]$_i$ steps (e.g., to 10 or 20 µM) capacitance rises after a lag, with a sigmoidal onset. We interpret the data in terms of a model similar to that of Thomas et al. (1993b). Based on this model, we find that the kinetics of calcium binding and unbinding to the secretory apparatus and of vesicle fusion are not sufficient to account for the persistence of secretion observed after termination of voltage depolarizations.

MATERIALS AND METHODS

Cell preparation and patch-clamp recording conditions

Chromaffin cells from bovine adrenal glands were prepared and cultured as described by Zhou and Neher (1993). Cells were used 1–4 days after preparation. The external bathing solution for experiments contained 150 mM NaCl, 2.8 mM KCl, 2 mM CaCl$_2$, 1 mM MgCl$_2$, 10 mM Hepes-NaOH, and 2 mg/ml glucose (pH 7.2, 320 mosm). Patch pipette solutions are described below. Conventional whole-cell recordings (Hamill et al., 1981) were per-

formed with 2–4 MΩ pipettes with resulting (uncompensated) series resistances of 5.9 ± 3.7 MΩ (mean ± SD). The membrane potential was held at −70 mV. All experiments were performed at room temperature (21–24°C).

Capacitance measurements

Two modes of capacitance measurements were employed. With the cell in the whole-cell configuration, capacitance was measured at low time resolution during most of the experiment by repetitive compensation of the cell capacitance using the CapTrack option of the EPC-9 patch clamp amplifier (Heka Elektronik, Lambrecht, Germany). Beginning 0.5 s before and continuing 4.5 s after an ultraviolet (UV) flash, the repetitive capacitance compensation of the EPC-9 was halted, and compensation was maintained at the last measured value. Further changes of capacitance above this value were measured with a software lockin: a 1600-Hz, 50-mV peak-to-peak sine wave was generated by an ITC-16 multichannel interface (Instrutech, Inc., Elmont, NY) controlled by a Macintosh Quadra700 computer running IGOR (WaveMetrics, Inc., Lake Oswego, OR) and Pulse Control XOPs (Jack Herrington and Richard Bookman, University of Miami, Coral Gables, FL). Neutralization of the bulk of the cell capacitance by the EPC-9 allowed the use of higher gains (e.g., 20 mV/pA) of the patch-clamp amplifier when operating the software lockin. To reconstruct the total cell capacitance and series resistance, the values of neutralized capacitance and measured series conductance were converted to equivalent real and imaginary components of the complex admittance based on the three-element model described in Lindau and Neher (1988) and added to the lockin real and imaginary outputs. Then the equations for the assumed three-element circuit were solved to obtain the values of membrane capacitance and series resistance.

The software lockin provided one capacitance point per sine wave period. We tested the response time of our capacitance measurement system by using a model circuit composed of a reverse-biased diode (which acts as a voltage-variable capacitor; Horowitz and Hill, 1989) in series with a resistor. A voltage of −70 mV was applied to maintain reverse bias. The software lockin was started with settings identical to those used in our experiments (50 mV peak-to-peak, 1600 Hz) and then a voltage step to −20 mV (i.e., a 50-mV step) was applied. The bulk of the diode capacitance (about 30 pF) was neutralized carefully such that current transients during such a step were minimized. The capacitance change, which should occur on the time scale of microseconds, was resolved as a "step" change (the capacitance sample interval was 620 μs, and the capacitance attained a new value within one data point; data not shown), indicating that the measurement system does not introduce artificial slowing in the capacitance records. This is important, as some of the capacitance changes we measured had time constants of about 1 ms, such that only a few points are found in the rising phase of the capacitance record.

Flash photolysis of caged Ca²⁺ and [Ca²⁺]ᵢ measurements

Flashes of UV light, derived from a Xenon arc flash lamp (Gert Rapp Optoelektronik, Hamburg, Germany) were coupled through a Schott UG11 filter to the epifluorescence illumination system of an Axiovert 10 microscope (Zeiss, Oberkochem, Germany) by means of a sapphire window (Steeg and Reuter, Gießen, Germany) placed at a 45° angle to the light path. This device combined the excitation light (alternating 350 and 390 nm) for fura-2 fluorescence, reflected at 15% efficiency, with the light from the flash lamp that passes straight through with 85% transmission. The fura-2 excitation light was provided by a two-flash lamp system (T.I.L.L. Photonics GmbH, Gräfelfing, Germany). The aperture stop of the microscope was set so that an area of ~70 μm diameter was illuminated. The cell under study was located in the center of this illuminated area. A circular sub-area of ~20 μm diameter that contained the cell was imaged onto a measuring photodiode (Model 9601, AME, Norway) for fluorescence measurement. The detection light path contained a 470-nm long-pass (Zeiss) and a 540-nm short-pass filter (Ditric Optics, Hudson, MA). The fura-2 excitation light intensity ("reference") was measured with a second photodiode (Type SFH,

Siemens, München, Germany). Fluorescence and reference signals were simultaneously integrated (ACF2101, Burr Brown, Tucson, AZ) and then digitized.

We used DM-nitrophen, tetrasodium salt, Calbiochem, La Jolla, CA) to release calcium, and furaptra (Molecular Probes, Eugene, OR) (Konishi et al., 1991) to measure calcium, as described by Neher and Zucker (1993) with the modifications here described. Since in this study we coupled the flash light to the epifluorescence illumination pathway of the microscope, we could confine the illumination to the cell and a 70-μm diameter field surrounding the cell. Thus, only a 30-μm section of the pipette was illuminated. This implied that only a small portion of DM-nitrophen in the pipette was photolyzed and that unphotolyzed DM-nitrophen from outside the field of illumination would rapidly diffuse back into the cell. Thus, [Ca²⁺]ᵢ changes were not step-like, but rather, rapid jumps to elevated levels followed by a slow decay, as shown in Fig. 1. Time constants of decline on average were 20.1 ± 7.7 s (mean ± SD). We also used a higher concentration of furaptra (1 mM) in this study to reduce the effects of flash-induced
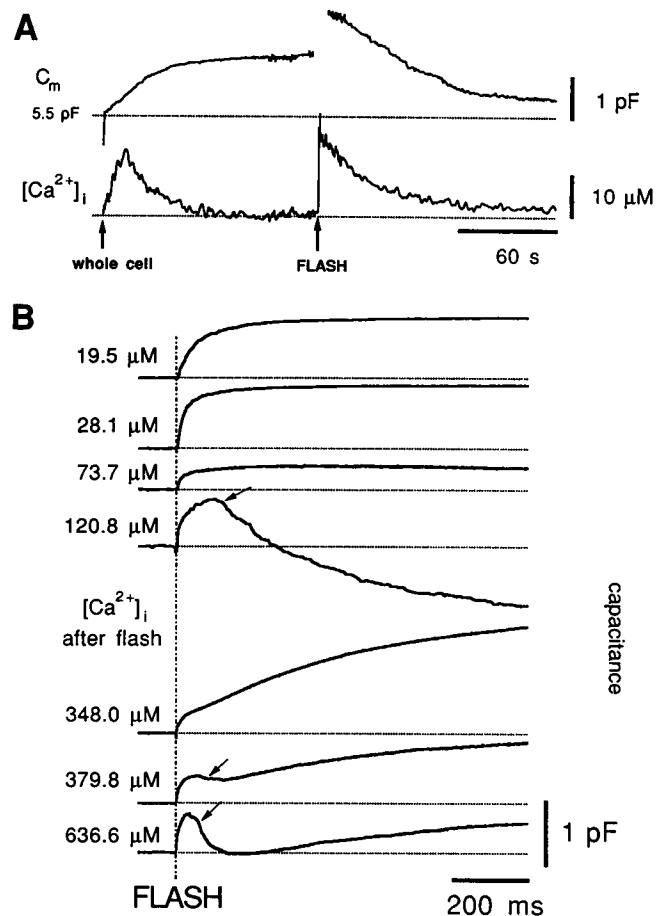

FIGURE 1 (A) Recording of an experiment with slow time resolution. After establishing the whole-cell configuration (first arrow) a loading transient led to a capacitance increase of 1.5 pF. During the loading transient the furaptra reading was not reliable due to the presence of Mg²⁺. At the time of the second arrow a UV flash increased [Ca²⁺]ᵢ to 19.5 μM. The rapid rise in [Ca²⁺]ᵢ increased the capacitance by 1 pF (see upper trace of Fig. 1 B). In the following 2–3 min a slow endocytotic process reduced Cₘ almost to its value at the beginning of the experiment. (B) Examples of secretory responses due to elevation of [Ca²⁺]ᵢ to different levels recorded at high time resolution. After the flash, in all examples shown, a double-exponential rising phase can be seen. The rate of rise in Cₘ increases with increasing [Ca²⁺]ᵢ steps. At higher [Ca²⁺]ᵢ indications for fast endocytotic process can be seen as a secondary decline in Cₘ (arrows). A pronounced slow component of Cₘ rise in the later part of the record was observed at high [Ca²⁺]ᵢ.

changes in DM-nitrophen fluorescence on the $[Ca^{2+}]_i$ measurement (Zucker, 1992). Composition of the intracellular solutions are shown in Table 1. The pH and the osmolarity of the solutions were adjusted to 7.2 and 320 mosm, respectively.

For calibration of the Ca^{2+} measurement we used the following procedure. The photolysis efficiency of the flash lamp was measured on droplets of 10–15 μm diameter in octanol. 4 μl of solution A (Table 1) and 80 μl octanol were mixed in a small cup. By shaking the mixture vigorously by hand for 2–5 s we got an emulsion with droplets of the desired diameter. The emulsion was put directly into the measuring chamber. The fura-2 fluorescence ratio was recorded from a single droplet. After recording of a baseline, photolysis flashes (175–375 V discharge, 20% neutral density (ND) filter) were given at 10-s intervals. The first few flashes did not change the fluorescence ratio significantly, because released Ca^{2+} was rapidly rebound to unphotolyzed DM-nitrophen, which was initially in excess. If more than 50% of the DM-nitrophen was photolyzed, the released Ca^{2+} exceeded the amount that could be rebound. Then the fura-2 fluorescence ratio would typically saturate within 1–3 flashes. With Eq. 6 from Zucker (1993a) one can calculate the photolysis efficiency of a flash for Ca^{2+}-free and Ca^{2+}-bound DM-nitrophen. A maximal flash in our system photolyzed 60% of Ca^{2+}-bound and 24% of Ca^{2+}-free DM-nitrophen.

Determination of the calibration constants for furaptra was performed by dialyzing cells with solutions B (R_{min}), C (K_{eff}), and D (R_{max}). After loading of the cells (1–2 min after going whole-cell) a maximal flash was given. R_{min} ($R_{min} = 0.363$) did not change significantly due to the flash. In cases where solutions C and D were dialyzed into the cells, a flash changed the fluorescence ratio not only because $[Ca^{2+}]_i$ changes, but also because DM-nitrophen and the furaptra bleach. By knowing the amount of released Ca^{2+} and assuming a tight 1:1 complex of the remaining unphotolyzed DM-nitrophen, a Ca^{2+} dissociation constant of 81 μM for (1, 3-diaminopropane-2-ol-N, N'-tetraacetic acid (DPTA), 250 μM for the nitrosoacetophenone-substituted iminodiacetic acid photo product of DM-nitrophen photolysis (Neher and Zucker, 1993), and 50 μM for furaptra we calculated the free $[Ca^{2+}]_i$ immediately after the flash. Using the calculated free Ca^{2+} concentrations before and after the flash of solutions C and D the calibration constants K_{eff}, R_{max}, $K_{eff}*$, and $R_{max}*$ (* indicates constants after the flash) were determined by two equations of the following form (Grynkiewicz et al., 1985):

$$[Ca^{2+}]_i = K_d \frac{R - R_0}{R_1 - R}. \tag{1}$$

The changes of the calibration constants for a maximal flash were as follows: $K_{eff} = 1.709$ mM to $K_{eff}* = 2.119$ mM and $R_{max} = 6.754$ to $R_{max}* = 6.679$. Calibration constants for photolysis efficiencies between 0 and 60% were estimated by linear interpolation of the above given values.

For experiments, cells were dialyzed with solution E (Table 1). DPTA was included at different concentrations to enable more controlled elevation of free Ca^{2+} concentration to levels over a wide range. The basal free Ca^{2+} concentration was between 300 and 600 nM as determined in experiments in which fura-2, instead of furaptra, was added to the pipette filling solution (fura, but not furaptra, can be used to measure calcium concentration in this low range). The fluorescence ratio of furaptra at this $[Ca^{2+}]_i$ was not distinguishable from its value of R_{min}. The calculation of the free Ca^{2+} con-

centration immediately after the flash was done according to Eq. 1 by adding the difference in the fluorescence ratio ($\Delta R = R_{after\ flash} - R_{before\ flash}$) to the mean ratio before the flash ($R_{min} = 0.363 \pm 0.001$, mean $\pm$ SD). With this procedure we avoid errors due to variability in the reading of R_{min}.

Kinetic analysis

The first-order differential equations derived from the reaction scheme (see below) were solved numerically, using a finite-difference approximation (first-order Euler scheme). The following parameters were used for all the calculations:

$$A = 5000\ \text{fF} \qquad k_1 = 0.009\ \text{s}^{-1} * [Ca^{2+}]/(1.2\ \mu\text{M} + [Ca^{2+}])$$

$$k_{-1} = 0.01375\ \text{s}^{-1} \qquad k_2 = k_{-2} = 1\ \text{s}^{-1} \qquad \gamma = 1000\ \text{s}^{-1}\ \text{or}\ 100\ \text{s}^{-1} \tag{2}$$

The parameters A and k_1 were taken from Heinemann et al. (1993) and the values of k_{-1}, k_2, and γ were modified or set as described in Results. Initial pool sizes for a given basal $[Ca^{2+}]_i$ were calculated for steady-state conditions, fixing A to 5000 fF. The free $[Ca^{2+}]_i$ used for model calculations was measured in a 1–2-s window following a flash. Simulations were conducted on a Macintosh computer with the IGOR program (WaveMetrics, Inc., Lake Oswego, OR).

RESULTS

Multiple components in the capacitance response to single flashes

Fig. 1 A shows a typical time course for $[Ca^{2+}]_i$ and capacitance during an entire experiment, displayed at low time resolution. The whole-cell recording configuration was established at the time indicated by the arrow (Fig. 1 A). In the subsequent 60–100 s a loading transient occurred, as described by Neher and Zucker (1993), which was due to cellular Mg^{2+} competing with and displacing Ca^{2+} bound to DM-nitrophen entering the cell. The increase in capacitance indicates that some secretion occurred. $[Ca^{2+}]_i$ dropped back to baseline as Mg^{2+} dialyzed out of the cell, and the capacitance climb leveled off. The baseline $[Ca^{2+}]_i$ was slightly elevated (in the range of 300–600 nM, as determined by fura-2 in a number of control experiments), which leads to optimal refilling of the pool of readily releasable vesicles (Neher and Zucker, 1993; Heinemann et al., 1993; von Rüden and Neher, 1993).

At about 140 s, a flash was given (375 V discharge, 20% ND filter), which photolyzed 12% of the Ca^{2+}-bound DM-nitrophen, according to the calibration given in Materials and Methods. It transiently increased $[Ca^{2+}]_i$ to 19.5 μM, after which $[Ca^{2+}]_i$ dropped back to baseline with a time constant of 30 s. Membrane capacitance (C_m) first rapidly increased by 1000 fF and later decreased due to endocytosis (see below). The time course of the increase is not illustrated in Fig. 1 A, because during the 5 s around the flash the alternate fast capacitance recording mode (see Materials and Methods) was active. An illustration of the fast events around the time of the flash is given in the upper trace of Fig. 1 B.

Seven examples of capacitance responses from different cells at higher time resolution for different flash intensities and $[Ca^{2+}]_i$ are shown in Fig. 1 B. In each example the responses have multiple-exponential time courses. There is a brief, rapidly rising phase within the first 100 ms after the

flash. This is the previously unresolved ultrafast phase of Neher and Zucker (1993) and is equivalent to the exocytotic burst described by Thomas et al. (1993a) in melanotrophs. This phase has been attributed to the fusion of vesicles from a small, readily releasable pool that becomes rapidly depleted. The initial rate of rise increases with $[Ca^{2+}]_i$. At low $[Ca^{2+}]_i$ an initial sigmoidal rising phase can be resolved (for higher time resolution see Figs. 2 and 4). At high $[Ca^{2+}]_i$ the beginning of a fast response (time constant 1–5 s; Neher and Zucker, 1993) can be seen (lower traces in Fig. 1 *B*), starting after the exocytotic burst; however, the amplitudes and time constants of this component are probably underestimated in this study, because $[Ca^{2+}]_i$ does not remain at a constant level after the initial flash-induced jump, due to the mixing of photolyzed cell and unphotolyzed pipette contents. For the same reason the slow response (time constant of minutes) of Neher and Zucker (1993) is not faithfully recorded in our experiments. A few of the traces show a secondary decline of capacitance, particularly at high $[Ca^{2+}]_i$ (Fig. 1 *B*, arrows). This is a clear indication of endocytosis.

Fig. 2 shows how we analyzed the secretory response after the flash. We concentrated almost exclusively on the ultrafast responses or exocytotic bursts. For each capacitance trace, we fitted the time course following the initial sigmoidal rising phase (delay) with either a single or a double exponential (at this stage of the analysis the delay was not included in the fit). For most responses a double exponential was required, but in some experiments, especially at $[Ca^{2+}]_i > 40$ μM, a single exponential was sufficient (Fig. 2). At low

$[Ca^{2+}]_i$ (< 5 μM) it was sometimes not possible to distinguish between the two components because both had slow kinetics. Three examples are given in Fig. 2, two of which required two exponentials. One was well fitted with a single exponential.

Recognition and separation of the fast and slow components was sometimes complicated by the onset of endocytosis. The degree of interference of the analysis by endocytosis was difficult to assess, especially because the amount of endocytosis is quite variable among cells. Thomas et al. (1994) have shown, however, that in melanotrophs endocytosis starts with a delay and that the fastest component of exocytosis is only little affected. Endocytosis in chromaffin cells also appears to start with a delay, as will be discussed further below (in the Rapid Endocytosis section).

Fig. 3 *A* shows how $[Ca^{2+}]_i$ affects the rate constants (reciprocal value of the time constants) of the exponential fits. Diamonds represent those cases in which two exponentials could be distinguished; ◆ corresponds to the first component (fast), and ◇ to the second component (slow) of ultrafast responses or exocytotic bursts. In response to weak flashes all cells showed two components. In most cells both components were also evident with $[Ca^{2+}]_i$ elevations to higher concentrations. The rate constants of the two components are separated by an order of magnitude. In other cells only one component (a slow single exponential), indicated by *, was observed. ○, △, and □ represent pooled averages of the first and second components, and of responses with only one component, respectively. Interestingly, in cases of only one component the rate constants fall into the band of the second (slower) component of responses in which a double exponential was required. At $[Ca^{2+}]_i > 40$ μM we fitted 23 responses with a double-exponential and 20 with a single-exponential function. Despite considerable scatter, it is seen that the rate constants of both components increase with $[Ca^{2+}]_i$ over two to three orders of magnitude before they saturate at about 1000 s^{-1} (first component) and below 100 s^{-1} (second component).

In Fig. 3 *B* maximal rates of secretion are plotted against $[Ca^{2+}]_i$. Maximal rates of secretion $\Delta C_m/\Delta t$ (not to be confused with the rate constants analyzed above, which presumably represent the rates of depletion of functional pools of vesicles) were measured following the sigmoidal onset (delay) of the capacitance response. Δt was set to half the fastest time constant analyzed in the exponential fit of the cell. The rates of secretion increase over three orders of magnitude and reach values of about 100,000 fF/s (40,000 vesicles/s) and about 10,000 fF/s (4000 vesicles/s) for double- and single-exponential responses, respectively. △ represents data from experiments using ionomycin-induced Ca^{2+} transients to elicit secretion as described by Augustine and Neher (1992). Despite the different methods used to elicit secretion (Ca^{2+} release from internal stores or from caged compounds), the secretory rates are similar, for similar $[Ca^{2+}]_i$.

The amplitudes of each exponential component of the exocytotic burst were fairly consistent for $[Ca^{2+}]_i > 10$ μM and
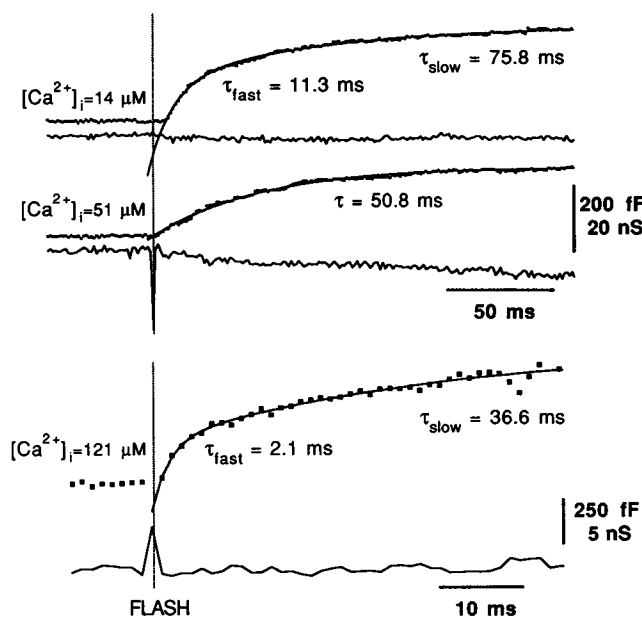
FIGURE 2 Analysis of the different kinetic components following a flash. Shown are the rising phases of C_m (dotted lines) after step elevation of $[Ca^{2+}]_i$ to the indicated values. Superimposed are exponential fits (solid lines) with their time constants. Usually a double exponential was required to fit the C_m trace, but sometimes (especially at high $[Ca^{2+}]_i$) a single exponential was sufficient (middle traces). In the upper trace a delay between the flash and the onset of the C_m rise was resolved. Series conductance (G_s) traces (solid lines) are not changing significantly after the flash.
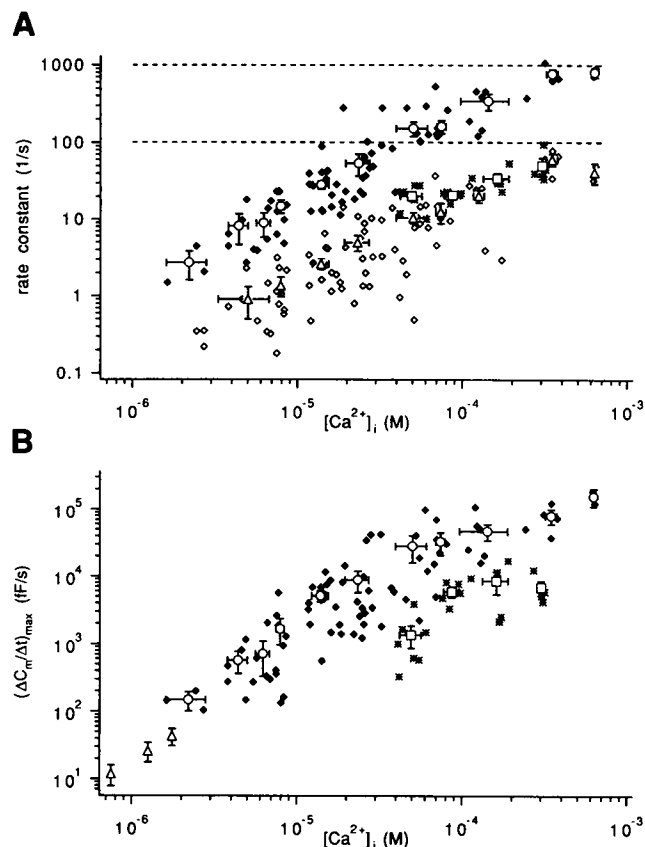
A

B

FIGURE 3 Ca^{2+} dependence of the different kinetic components. (A) Rate constants versus $[Ca^{2+}]_i$. Responses that had a double-exponential rising phase are shown as diamonds. The first component ($\blacklozenge$) is about one order of magnitude faster than the second component ($\lozenge$). (O,$\triangle$) Pooled averages of the first and second component, respectively. Averaged values are given $\pm$SE (ordinate) and $\pm$SD (abscissa). (*) Responses with only one exponential component; ($\square$) pooled averages of these responses, which have rates comparable with the second component of double-exponential responses. At high $[Ca^{2+}]_i$ the rates of the first and the second components saturate at about 1000 and 100 s^{-1}, respectively (dashed lines). (B) Maximal rates of C_m increase versus $[Ca^{2+}]_i$. ($\blacklozenge$) maximal rates of C_m increase of the first component (compare Fig. 3 A). (*) Maximal rates of C_m increase of responses where only one component was present. Pooled averages for maximal rates of secretion of double- and single-exponential responses are shown as O and $\square$, respectively. The maximal rates of the single-exponential responses are about one order of magnitude smaller than the maximal rates of secretion analyzed in double exponential responses. Pooled averages of rates of secretion from four experiments with ionomycin-induced $[Ca^{2+}]_i$ elevations taken from Augustine and Neher (1992) are shown as $\triangle$.

had average values of 251 $\pm$ 26 fF (n = 57, mean $\pm$ SE) (first component of the double-exponential response), 273 $\pm$ 25 fF (n = 57) (second component of the double-exponential response), and 253 $\pm$ 35 fF (n = 22) (single-exponential response).

At $[Ca^{2+}]_i \geq 100$ μM, we observed in 15 of 21 experiments a slower kinetic component (see Fig. 1 B) similar to the fast component described by Neher and Zucker (1993). The amplitude of this component was 1003 $\pm$ 143 fF (mean $\pm$ SE, n = 15) at $[Ca^{2+}]_i$ of 322 $\pm$ 145 μM (mean $\pm$ SD). As mentioned earlier, the amplitude of this slow component was underestimated in our experiments because of overlap of

endocytotic processes and gradual exchange of pipette and cell calcium and buffers.

Kinetic modeling of the exocytotic burst

As noted in the Introduction, our goal is to understand the time course of secretion during electrical stimulation of the cells, particularly after termination of a depolarizing voltage step. This can be done only in the framework of a kinetic model. Unfortunately our data are too complex to be described in full by a single reasonable model. In particular, the overlap of exocytosis and endocytosis prevents a complete quantitative description of the late time course of flash responses, at least until the kinetics of endocytosis are better understood. Nevertheless, we will make an attempt here to explore what constraints the early time course of flash responses puts on the time course following a depolarization.

Scheme 1
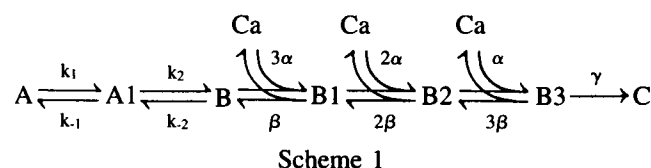
We restrict this analysis to sequential models such as those used by Heinemann et al. (1993), Neher and Zucker (1993), and Thomas et al. (1993b). Our starting point is the two-step model of Heinemann et al. (1993), a model that successfully fits experimental findings in chromaffin cells for secretion stimuli that raise $[Ca^{2+}]_i$ more slowly and to lower levels than flash experiments (see also von Rüden and Neher, 1993). We extend this model (see Scheme 1) by including an additional pool of vesicles (A1), located between pools A (reserve pool) and B (readily releasable pool). Pool A1 contributes the slower component to the double-exponential ultrafast response or exocytotic burst. The rapid processes of Ca binding and secretion are represented by a sequence of three Ca-binding steps followed by an irreversible secretion step with rate constant γ (see also Thomas et al., 1993a). The designation of the binding (forward) rate constants as 3α, 2α, and α in successive steps (and the corresponding dissociation (reverse) rate constants as β, 2β, 3β) simulates independent (i.e., noncooperative) Ca^{2+} binding to three sites, in a manner analogous to models of independent "gating-particle" movements in ionic channel gating (e.g., Armstrong, 1969). (Although we assume here independent and equal binding to each site, the model can accommodate more complicated, "cooperative" binding.) Vesicles appearing in pool C contribute to membrane capacitance, such that the increase in pool C should be directly proportional to the increase in membrane capacitance C_m (not to be confused with pool C), as long as no endocytosis takes place. It should be noted that what is generally termed "secretion rate" is proportional to the derivative of pool C or membrane capacitance.

We analyzed the responses of the model to step increases in $[Ca^{2+}]_i$ over a period of ~500 ms following the step. Before a simulated flash, a resting $[Ca^{2+}]_i$ level was specified (as noted in Materials and Methods, the actual preflash basal $[Ca^{2+}]_i$ could not be measured routinely, as furaptra was used

in experiments), and the the number of vesicles in each of the pools A, A_1, and B in Scheme 1 was allowed to reach equilibrium. For example, for resting $[Ca^{2+}]_i = 100$ nM and $k_1 = 6.9 \times 10^{-4}$ s^{-1} (Heinemann et al., 1993), $k_{-1} = 0.01375$ s^{-1} (von Rüden and Neher, 1993) and both k_2 and $k_{-2} = 1$ s^{-1}, pool B at steady state contains 100 vesicles (2.5 fF/vesicle). We could have made the initial pool size adjustments alternatively by fixing the basal $[Ca^{2+}]_i$ to a desired level and varying the size of pool A, but the result would have been the same with regard to size and kinetics of the exocytotic burst.

The model predicts that a step of $[Ca^{2+}]_i$ to high levels (e.g., to 100 μM) will lead to an exocytotic burst, with an approximately double-exponential ultrafast phase. The faster exponential component will have a time constant of about $1/\gamma$. For lower concentrations, the early response will display a sigmoidal rising phase due to the kinetics of the Ca^{2+}-binding/unbinding step. In addition, the rate constants α and β will be related to one another in a fixed ratio, the K_d ($= \beta/\alpha$), which gives an indication of the affinity of Ca^{2+} to one of its multiple binding sites (each identical in the present model).

Below we explore different versions of the model assuming different maximum secretion rates γ (100 or 1000 s^{-1}) and also different numbers of Ca^{2+}-binding steps (two, three, or four ions binding). In each case we determine what constraints the measured time course puts on the selection of α and β. It should be noted that the choice of parameters concerning states A and A_1 and the slow transition between them influences the ultrafast time course very little, except for setting the amplitude of the second (slower) exponential component, which shows up as a sloping baseline with a time constant in the range of 500 ms (set by k_2 and k_{-2})).

For the choice of γ we noted that at $[Ca^{2+}]_i > 40$ μM we could distinguish responses with single- or double-exponential time courses. The time constants of the faster component for the cases fit with double exponentials were about an order of magnitude faster than those of the single-exponential time courses ($\sim$1000 compared with 100 s^{-1}, respectively). Thus, the cells appeared to belong to one of two kinetic classes. At lower concentrations we observed, as a rule, a slower double-exponential response, and we had no means to distinguish to which class a given cell belonged. Therefore, we analyzed each cell six times, assuming two, three, or four Ca^{2+}-binding sites and using either 100 or 1000 s^{-1} for γ.

If there are two classes of cells that differ only in having a fast or slow final rate-limiting step, then fits with the "correct" γ should yield constant values for α and β, regardless of the calcium concentration. As will be shown below (Fig.4), in such a case a plot of α versus β for points at different $[Ca^{2+}]$ will give a compact cluster of points. On the other hand, "incorrect" assignments of γ will lead to erroneous estimates of α and β, and plots of α versus β will show considerable scatter.

We selected 21 representative traces in the $[Ca^{2+}]_i$ range between 3 and 30 μM for detailed kinetic analysis. All of the

examples at this relatively low $[Ca^{2+}]_i$ showed delays. In each case, we assigned γ to either 1000 or 100 s^{-1} and then adjusted α and β by trial and error until the calculated capacitance time course matched the observed capacitance time course. The amplitudes of the simulated capacitance increases were adjusted by varying the pre-flash basal $[Ca^{2+}]_i$, which influenced the initial pool sizes.

Fig. 4 A shows an example of a fast analysis ($\gamma = 1000$ s^{-1}) with simulations based on models having two, three, and four Ca^{2+}-binding steps. The overall experimental time course (left panel, solid lines) was reasonably well fitted by all three models (superimposed broken lines). Closer inspection of the onset of the response (right panels) immediately after the flash shows that a model with four Ca^{2+}-binding steps has a more pronounced sigmoidicity than a model with two Ca^{2+}-binding steps. However, from an individual fit it was not possible to exclude any particular stoichiometry.

In Fig. 4 B we show a summary of all the fits. In the top row the plots show α versus β from fits in which γ was assigned arbitrarily for the entire set of selected cells to either 100 (*) or 1000 s^{-1} (O). The left, middle, and right plots show results when the model had two, three, and four Ca^{2+}-binding steps, respectively. There is considerable scatter, particularly in the values of α, perhaps due to the "incorrect" classification of cells with regard to the rate constant γ. After assigning 13 responses to the fast class and 8 responses to the slow class, the plots show far less scatter (compare top and bottom rows of Fig. 4 B). The ratio of fast class to slow class responses of 13/8 is close to the ratio of 23/20 observed at high $[Ca^{2+}]_i$. The mean of the off-rate β is not much affected either by the value of γ nor by different Ca^{2+} stoichiometries (see Fig. 4 B and Table 2), whereas αs depend more strongly on the assumptions made. In Table 2 mean parameters are summarized for the two classes and the three different Ca^{2+}-binding stoichiometries. Inspection of Table 2 reveals that when $\gamma = 1000$ s^{-1} is used for fast responses and $\gamma = 100$ s^{-1} for slow responses, quite consistent estimates of α and β (and consequently the Ca^{2+} dissociation constant ($K_d(Ca^{2+})$) of the reaction triggering exocytosis) are obtained for all responses, for any assumed Ca^{2+} stoichiometry.

It should be pointed out that the assignment of cells to two distinct kinetic classes in the low-concentration range is not necessarily inconsistent with the observation at high concentration that the slow class is well described by a single-exponential time course, because we cannot exclude the possibility that cells showing single-exponential responses at high $[Ca^{2+}]_i$ may show double exponentials at low $[Ca^{2+}]_i$.

To compare the results of the individual fits with our experimental results over the full range of $[Ca^{2+}]_i$ studied, we calculated the maximal rate of secretion using the averaged parameters from the fits. In Fig. 5 the calculated maximal rates of secretion (lines) for the fast class are superimposed on the experimental results. The responses selected to estimate the parameters are indicated in Fig. 5 (*). At $[Ca^{2+}]_i > 10$ μM the model predictions for all different Ca^{2+} stoichiometries are in good agreement with the experimental results. At lower $[Ca^{2+}]_i$, however, the calculated maximal rates of
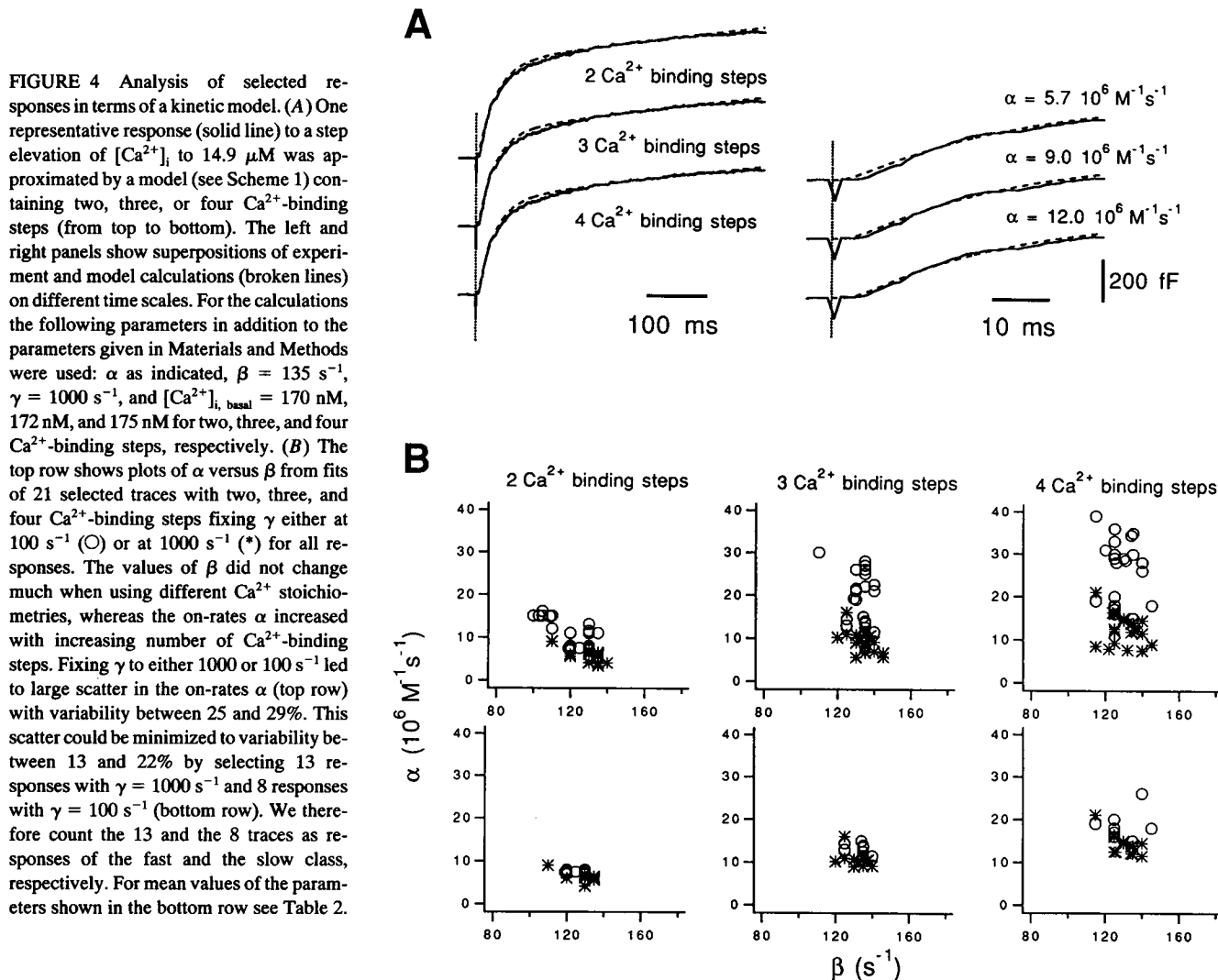
FIGURE 4 Analysis of selected responses in terms of a kinetic model. (A) One representative response (solid line) to a step elevation of $[Ca^{2+}]_i$ to 14.9 μM was approximated by a model (see Scheme 1) containing two, three, or four Ca^{2+}-binding steps (from top to bottom). The left and right panels show superpositions of experiment and model calculations (broken lines) on different time scales. For the calculations the following parameters in addition to the parameters given in Materials and Methods were used: α as indicated, $\beta = 135$ s^{-1}, $\gamma = 1000$ s^{-1}, and $[Ca^{2+}]_{i, \text{ basal}} = 170$ nM, 172 nM, and 175 nM for two, three, and four Ca^{2+}-binding steps, respectively. (B) The top row shows plots of α versus β from fits of 21 selected traces with two, three, and four Ca^{2+}-binding steps fixing γ either at 100 s^{-1} (O) or at 1000 s^{-1} (*) for all responses. The values of β did not change much when using different Ca^{2+} stoichiometries, whereas the on-rates α increased with increasing number of Ca^{2+}-binding steps. Fixing γ to either 1000 or 100 s^{-1} led to large scatter in the on-rates α (top row) with variability between 25 and 29%. This scatter could be minimized to variability between 13 and 22% by selecting 13 responses with $\gamma = 1000$ s^{-1} and 8 responses with $\gamma = 100$ s^{-1} (bottom row). We therefore count the 13 and the 8 traces as responses of the fast and the slow class, respectively. For mean values of the parameters shown in the bottom row see Table 2.

TABLE 2 Parameters estimated by fitting C_m responses with different Ca^{2+} stoichiometries and rate-limiting fusion steps

Number	Ca^{2+}	$\gamma = 1000$ s^{-1}			$\gamma = 100$ s^{-1}		
		α (10^6 M^{-1} M^{-1})	β (s^{-1})	K_d (μM)	α (10^6 M^{-1})	β (s^{-1})	K_d (μM)
2	fast	**6.4 ± 0.9**	**129 ± 8**	**20.6 ± 3.1**	13.3 ± 1.9	115 ± 12	8.9 ± 2.1
	slow	3.9 ± 0.3	134 ± 4	34.4 ± 3.1	**7.5 ± 0.4**	**124 ± 5**	**16.6 ± 1.1**
3	fast	**10.7 ± 1.8**	**132 ± 6**	**12.6 ± 1.9**	23.7 ± 3.5	132 ± 8	5.7 ± 0.9
	slow	6.9 ± 1.1	138 ± 5	20.3 ± 3.4	**13.4 ± 1.1**	**133 ± 5**	**10.0 ± 1.1**
4	fast	**14.3 ± 2.5**	**130 ± 7**	**9.4 ± 1.8**	31.7 ± 3.5	128 ± 7	4.1 ± 0.5
	slow	9.2 ± 1.8	130 ± 10	14.5 ± 2.9	**18.6 ± 3.4**	**129 ± 10**	**7.1 ± 1.2**

"Fast" ($n = 13$) and "slow" responses ($n = 8$) were approximated using Scheme 1 either with $\gamma = 1000$ s^{-1} or $\gamma = 100$ s^{-1} (for details see text). When $\gamma = 1000$ s^{-1} was used for fast responses and $\gamma = 100$ s^{-1} for slow responses (bold numbers), quite consistent estimates of α, β, and K_d are obtained for any assumed Ca^{2+} stoichiometry. Values are given as mean ±SD.

secretion using a model with two Ca^{2+}-binding steps are about one order of magnitude higher than the measured values. The predictions of the third- and fourth-power Ca^{2+} dependence describe the experimental results in a reasonable way over the entire $[Ca^{2+}]_i$ range studied. At low $[Ca^{2+}]_i$ they are also in good agreement with the predictions of the model published previously (solid line) and the data from ionomycin-induced Ca^{2+} transients ($\triangle$).

As indicated above, the ratio of off-rate to on-rate constants (β/α) represents the $K_d(Ca^{2+})$ of a single Ca^{2+}-binding site. Our analysis gives a $K_d(Ca^{2+})$ in the range between 9 μM (for four Ca^{2+} ions) and 13 μM (three Ca^{2+} ions) for cells of the fast class.

Using the kinetic scheme, we can now evaluate how much the rates of Ca^{2+} binding and unbinding and vesicle fusion contribute to the persistence of secretion after a depolariza-
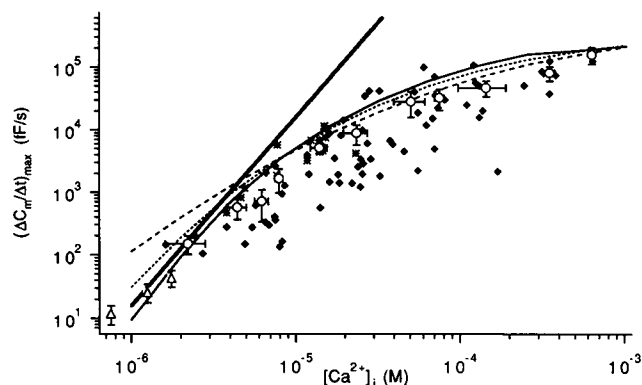
FIGURE 5 Comparison of the maximal rates of secretion with model predictions. ($\blacklozenge$,$\bigcirc$) maximal rates and their pooled averages from cells of the fast class (compare Fig. 3 B). (*) responses selected for determining parameters. ($\triangle$) maximal rates of C_m increase from experiments with ionomycin-induced elevation of $[Ca^{2+}]_i$. Model calculations were done using the mean values of the 13 fits that were identified as fast class responses (for parameters see bold printed numbers in the left panel of Table 2). For $[Ca^{2+}]_i > 10$ μM calculations with all three Ca^{2+} stoichiometries describe the data well. At $[Ca^{2+}]_i < 10$ μM, however, the calculation with two Ca^{2+}-binding steps (dashed line) gives rates that are about one order of magnitude too high. Models with three (dotted line) and four (thin solid line) Ca^{2+}-binding steps approximate the data also at low $[Ca^{2+}]_i$. The straight solid line gives maximal rates calculated with the model and parameters published by Heinemann et al. (1993). That model also describes our data at low $[Ca^{2+}]_i$. At high $[Ca^{2+}]_i$, however, a large discrepancy between the previous model and our data can be seen. This is due to the absence of a rate-limiting step leading to final fusion of the vesicle in the previous model.

tion ends. The rate of secretion depends on the number of vesicles in pool B3 (the pool of release-ready vesicles that are about to fuse) and the rate constant γ, according to the relationship

$$\frac{dC}{dt} = \gamma[B3] \qquad (3)$$

where C refers to the pool of fused vesicles in Scheme 1. The rate of change in the size of pool B3 depends, in turn, upon the sum of all the rates for entering and leaving state B3; the time constant would be the inverse of this rate. In the hypothetical case of a sudden drop of $[Ca^{2+}]_i$ to 0 at the end of an idealized rectangular calcium pulse, the size of B3 will decay away with a time constant of

$$\tau = \frac{1}{\gamma + s_j\beta}; \qquad s_j = 3, 4 \qquad (4)$$

For typical values of β and γ (Table 2), this time constant is in the range of about 0.7 (for the fast γ) to 2.0 ms (for the slow γ). The rate of secretion would also decay away at the same rate.

Rapid endocytosis

As seen in Fig. 1, we can distinguish at least two different endocytotic processes. One has a time constant in the tens of seconds to minutes range (see Fig. 1 A), and the other one is in the subsecond range (see Figs. 1 B and 6 A). We iden-
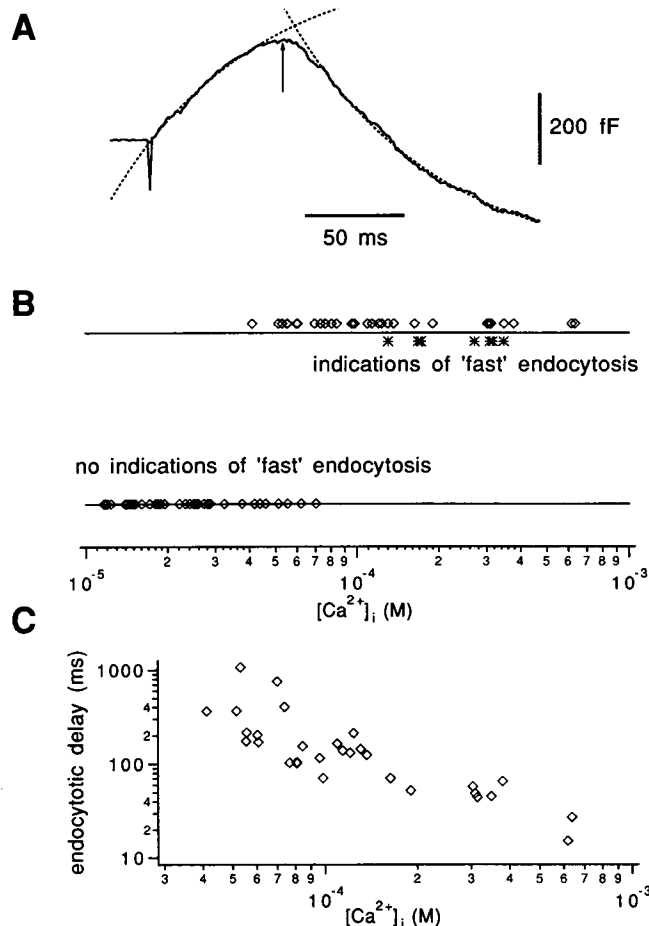

FIGURE 6 Ca^{2+} dependence of a fast endocytotic process. (A) A particularly prominent example of fast endocytosis. At the end of an exocytotic burst ($[Ca^{2+}]_i = 98.5$ μM) the fast endocytotic process overcomes exocytosis (arrow) and C_m starts to decrease rapidly. Data (solid line) are superimposed with single-exponential fits (broken lines) of the exocytotic burst and the onset of the endocytotic process. The time constants of the exponentials are 73.5 and 75.3 ms for the exocytotic and endocytotic process, respectively. (B) Ca^{2+} dependence of the probability that fast endocytosis was observed. In a time window of 2 s after the flash the experimental records were checked for a decline in C_m ($\Diamond$). At $[Ca^{2+}]_i < 40$ μM no decline was observed. At $[Ca^{2+}]_i > 40$ μM the probability that an indication of endocytosis was detected increased rapidly. (*) Responses where only a transient slowdown of the capacitance increase was observed; in these cases a pronounced slow phase of C_m increase was present. For an example, see third trace from the bottom in Fig. 1 B. (C) Ca^{2+} dependence of the endocytotic delay. The time between the flash and the earliest indication of endocytosis (onset of a negative slope in C_m) is plotted against the step elevation in $[Ca^{2+}]_i$. The endocytotic delay decreases with increasing step elevations in $[Ca^{2+}]_i$.

tified clear examples of endocytosis by searching for a negative slope in the capacitance trace in a time window of 2 s following the flash. In some experiments it was possible to fit the fast endocytotic process with a decaying exponential. Membrane was retrieved with time constants of 62 $\pm$ 14 ms (mean $\pm$ SE, $n = 6$) in response to $[Ca^{2+}]_i$ steps higher than 100 μM. In many cases endocytosis seemed to have an abrupt onset (Fig. 6 A) suggesting that the fast endocytotic process starts after a delay following Ca^{2+} elevation. We

therefore call the time between the flash and the onset of a negative slope in C_m endocytotic delay. In cases where a large slow exocytotic component was present, endocytosis often did not exceed exocytosis. In those cases only a transient slowdown of the capacitance increase was seen (see Fig. 1 B, third trace from the bottom).

Examples of endocytosis with sub-s time constants were much more common for $[Ca^{2+}]_i$ steps to higher than about 50 μM (see Fig. 6 B). Of course, endocytosis may occur also at lower $[Ca^{2+}]_i$, at rates that do not exceed exocytosis. In such cases, the overlap of exo- and endocytosis may not be readily discerned. The endocytotic delay decreased with increasing $[Ca^{2+}]_i$, becoming as short as 20 ms when $[Ca^{2+}]_i$ was about 600 μM (Fig. 6 C). If endocytosis starts simultaneously with exocytosis, then one would expect that the amplitude of the exocytotic burst (which is approximately constant for calcium concentrations above 10 μM in cells with no obvious endocytosis) would appear reduced in cases where clear endocytosis occurs, compared with those in which there is no obvious endocytosis. In fact, the size of the exocytotic burst is not reduced in cases with endocytosis (as in the case of melanotrophs, the size of the exocytotic burst in cases with clear endocytosis was often slightly larger than in cases without endocytosis), suggesting that endocytosis probably occurs with a delay lasting about as long as the exocytotic burst.

In some cases, the final capacitance attained after a flash was lower than that immediately before the flash (see fourth trace from the top in Fig. 1 B). However, in such cases, the final capacitance was nearly always close to the level measured at the time the whole-cell configuration was obtained, before the loading transient.

DISCUSSION

Multiple exocytotic components in bovine chromaffin cells

We have shown in bovine chromaffin cells that sudden elevations in $[Ca^{2+}]_i$ led to complex exocytotic responses and often to endocytosis as well. The initial exocytotic burst started with a Ca^{2+}-dependent delay and was followed by one or two exponential components having time constants as short as 1 ms and rates of secretion as high as 100,000 fF/s (for $[Ca^{2+}]_i > 100$ μM). The amplitudes of the first and second components added up to the same amplitude as the ultrafast response of about 0.5 pF measured by Neher and Zucker (1993). The Ca^{2+} dependence of the secretory rates during the exocytotic burst was measured in the $[Ca^{2+}]_i$ range between 3 and 600 μM (Fig. 3). At $[Ca^{2+}]_i > 100$ μM, in 68% of the experiments an additional component with slower kinetics was present. This component, termed "fast secretion" by Neher and Zucker (1993), was not seen at lower $[Ca^{2+}]_i$. This is in good agreement with the measurements by Neher and Zucker (1993).

Multiple endocytotic processes

In addition, endocytotic processes have been resolved. We distinguished a slow endocytotic process that recycles exocytosed membrane on the time scale of tens of seconds to minutes. This process seemed to be triggered by the amount of previously exocytosed membrane and not by $[Ca^{2+}]_i$. On the other hand there was a faster endocytotic process that reached time constants faster than 100 ms. This process sometimes retrieved more membrane than was added during the preceding exocytotic burst. The fast endocytosis is qualitatively similar to the excess retrieval measured by Thomas et al. (1994) in melanotrophs from the pars intermedia of rat pituitary. However, the time constant of the fast retrieval in chromaffin cells was about three times faster. Thomas et al. (1994) suggested that excess retrieval starts after a delay following elevation of $[Ca^{2+}]_i$, and that the delay lasts about as long as the exocytotic burst. Their findings together with our results that the decline in C_m starts very abruptly after the amplitude of the exocytotic burst has reached about 80% of its average value (sum of first and second components) make it unlikely that the analysis of the fast component of the exocytotic burst is confounded by this fast endocytotic process.

Kinetic model

We have interpreted our data in terms of the model shown in Scheme 1. This model, with three or four Ca^{2+}-binding steps, simulates the Ca^{2+}-dependent delay and the maximal rates of secretion quite successfully. To fit the data either with three or four Ca^{2+}-binding steps, a change only in the on-rate α of Ca^{2+} binding was necessary. The on-rate α was about an order of magnitude lower than the diffusion limit. When extrapolating predicted initial rates of secretion to lower $[Ca^{2+}]_i$, values quite close to those measured previously are obtained (Augustine and Neher, 1992; Heinemann et al., 1993; von Rüden and Neher, 1993).

The K_d of a single Ca^{2+}-binding site predicted by our model is between 7 and 13 μM (for Ca^{2+} stoichiometry of 3-4). There are several membrane-bound Ca^{2+}-binding proteins (CaBPs) with K_ds in that range (see review by Kasai, 1993). The $K_d(Ca^{2+})$ of the CaBP annexin I (Glenny et al., 1987) of 10 μM and synaptotagmin I (Brose et al., 1992; Bazbek and Südhof, 1994) of about 6 μM match our estimate best. Annexin I regulates chromaffin granule aggregation (Wang and Creutz, 1992); however, the kinetics of granule aggregation are slow (range of several minutes) compared with the exocytotic processes described here (sub-s range). Synaptotagmin is one of the leading candidates for the calcium sensor that triggers Ca^{2+}-dependent secretion (Jahn and Südhof, 1994). The protein has two calcium-binding regions, the so-called "C2 domains" that resemble portions of protein kinase C (Bazbek and Südhof, 1994).

In our model we assume identical Ca^{2+}-binding sites or the involvement of only one type of CaBP. A more complicated model with cooperativity or different CaBPs and different

K_ds could probably also describe the C_m responses. Our data were not sufficient to discriminate among the possibilities. Nevertheless, our model predictions give a rough estimate of the Ca^{2+} affinity of a single binding site. It should be noted that half-maximal rates of secretion (about 50,000 fF/s) are reached at $[Ca^{2+}]_i > 40$ μM. This is about four times higher than the estimated K_d for a single binding site. The binding of multiple Ca^{2+} ions and the rate-limiting step following Ca^{2+} binding account for the difference.

At high $[Ca^{2+}]_i$, there was an additional slower kinetic component present. This component was called the fast phase of secretion by Neher and Zucker (1993). Since $[Ca^{2+}]_i$ higher than 100 μM is needed to trigger this component, an additional Ca^{2+}-dependent step with a much lower affinity is needed to account for this component. On the other hand, prolonged stimulation with $[Ca^{2+}]_i < 2$ μM is sufficient to release all vesicles localized in pool A (Augustine and Neher, 1992). If the low-affinity step is located in series with pools A and B, it must supply vesicles with a rate between at least 20 and 40 fF/s for $[Ca^{2+}]_i$ in the range between 1 and 80 μM. Above 100 μM it must increase its rate and amplitude very rapidly. Since this is very unlikely, this step might be in parallel to steps A to B. This process could have a Ca^{2+} dependence that has a high threshold and needs $[Ca^{2+}]_i$ as high as that in the vicinity of a Ca^{2+} channel, but whose maximum rate is not as fast as the release of already-docked vesicles.

Our model includes a Ca^{2+}-dependent transport of vesicles between reserve pool A and pool A1 that leads to a Ca^{2+}-dependent priming of secretion (Bittner and Holz, 1992; Neher and Zucker, 1993; von Rüden and Neher, 1993). This transition in vesicle readiness for release might reflect changes in cytoskeletal proteins that influence the ability of vesicles to subsequently dock at membrane release sites (Trifaró and Vitale, 1993).

Maximum secretory rate

We observed maximum rates of secretion of about 100,000 fF/s or 40,000 vesicles/s on flash photolysis of DM-nitrophen. This is higher than previous estimates (Neher and Zucker, 1993), due to the higher temporal resolution of the present capacitance measurements. Assuming that about 200 vesicles (corresponding to 500 fF, which is equivalent to the size of a double-exponential exocytotic burst) are readily releasable, one calculates that a single vesicle is released at a rate of about 200 s^{-1}. This estimate, which is based on measured overall maximum rates is, as expected, intermediate between those derived from fitting exponentials to fast and slow components. At crayfish claw opener muscle neuromuscular junctions (Zucker, 1993b; L. Landó and R. Zucker, unpublished), flash photolysis of DM-nitrophen releases ~100 quanta/ms (100,000 quanta/s) at motor nerve terminals. An extracellular electrode records releases from about five release sites (Zucker, 1973) corresponding to about 2% of all motor nerve terminals (Bittner and Kennedy,

1970). This implies that a synapse consists of about 250 release zones with an area of about ¼ μm^2 each (Jahromi and Atwood, 1974), so release occurs from a membrane area of about 62.5 μm^2. If a quantum of transmitter release represents fusion of a single synaptic vesicle, and a release site contains one readily releasable vesicle, such a vesicle could be released with a rate constant of about 400 s^{-1}. This is only a factor of two faster than the release of a vesicle in chromaffin cells. On the other hand, due to structural specialization, synapses are able to secrete at a rate of 1,600 quanta/s/μm^2, whereas chromaffin cells reach only rates of 60 vesicles/s/μm^2 surface area. This is about 25 times slower than secretion from a synapse.

A recent model of secretion from neurons (Yamada and Zucker, 1992) is similar to the present model in that it includes sequential binding of multiple Ca^{2+} ions followed by a rate-limiting exocytotic step. In the neural model, release occurs with somewhat lower Ca^{2+} affinity, faster Ca^{2+}-binding/unbinding kinetics, and a faster rate-limiting secretion step following Ca^{2+} binding than in our model for chromaffin cells. These properties could account for the faster maximal rate of secretion in neurons.

Persistent secretion in chromaffin cells is not due to slow secretory machinery

Our analysis has helped to rule out sluggish secretory machinery as the explanation for the persistence of secretion after termination of a depolarizing stimulus. Secretion would be expected to continue after calcium levels dropped to basal if either secretion were obligatorily slow (i.e., γ slow) or unbinding of calcium from the fusion apparatus were slow (i.e., β slow). Neither appears to be the case, and, as summarized in Eq. 4, secretion should not persist more than 2–3 ms beyond the time that calcium levels decrease to basal, at least based on the kinetic properties of the fusion apparatus.

What are other possible explanations for the continued secretion? The period over which secretion persists is predicted to be much shorter if secretory vesicles and calcium channels are co-localized in chromaffin cells, as they appear to be in synapses (Robitaille et al., 1990; Cohen et al., 1991). In the case of such co-localization, secretion should stop within at most a few ms after termination of a depolarizing stimulus, as $[Ca^{2+}]$ near single Ca channels should drop to near-basal levels within 10's of μs of channel closure (Nowycky and Pinter, 1993). This is certainly the case for the neuromuscular junction of frog and crayfish (Katz and Miledi, 1965; Parnas et al., 1989). Thus, the prolonged secretion may indicate that at least some calcium channels and secretory vesicles are not co-localized. In such circumstances, the secretion kinetics would reflect the slower calcium time course due to a greater diffusion distance and due to the increasing influence of calcium buffering. We address this and other possible mechanisms in another paper (Chow, R. H., Klingauf, J., Heinemann, C., Zucker, R. S., and Neher, E., manuscript in preparation).

Time course of free calcium after flash photolysis of caged Ca^{2+}

Zucker (1993a) showed in in vitro experiments that a UV flash of DM-nitrophen-containing solutions can generate a large (10's or 100's of μM) transient increase of $[Ca^{2+}]_i$ of ms duration (a "spike") at the leading edge of a step-like increase in $[Ca^{2+}]_i$ when total DM-nitrophen exceeds the total Ca^{2+}. This was attributed to the relatively slow Ca^{2+} rebinding to unphotolyzed DM-nitrophen compared with the fast photolytic release of Ca^{2+}. In the present experiments, we used 10 mM DM-nitrophen, 10 mM Ca^{2+}, and mM amounts of the calcium buffer DPTA. With fully Ca^{2+}-saturated DM-nitrophen, whether or not there is a significant Ca^{2+} spike depends on whether the on-rates for Ca^{2+} binding to endogenous buffers and to DPTA are slower than the rate of photolytic Ca^{2+} release. We have performed simulations of the Ca^{2+} time course for solutions (cf. Zucker, 1993a) containing 10 mM Ca^{2+}-saturated DM-nitrophen, 10 mM DPTA (assuming an on-rate of $10^7 M^{-1} s^{-1}$, similar to EGTA, as there are no published values for the on-rate of DPTA), and 0.4 mM of a buffer with a $K_d(Ca^{2+})$ of 10 μM and $10^7 M^{-1} s^{-1}$ on-rate (the "endogenous" fixed calcium buffer; see Zhou and Neher, 1993). If a flash were applied to raise $[Ca^{2+}]_i$ to a step level of 15 μM, there should be a Ca^{2+} spike to 80 μM for about 1–2 ms. Such spikes with peak $[Ca^{2+}]_i$ about five to six times higher than the equilibrated step elevation would significantly accelerate the early rise (first 10 ms) of our modeled C_m responses. Experimentally, we find that C_m increases only slowly (sigmoidal rise) or not at all in this time window. A simple reduction of the on-rate in our model for secretion (Scheme 1) cannot eliminate an expected sudden rise in C_m right after the flash.

Similarly we simulated the conditions of the experiments of Neher and Zucker (1993): flash photolysis of 8.5 mM DM-nitrophen loaded with 3 mM Ca^{2+} in a cell should produce a Ca^{2+} spike of 60 μM. According to our model such a spike should produce about 100 fF secretion. However, no such increase in C_m was detected by Neher and Zucker (1993). Our results, therefore, suggest that the submembrane Ca^{2+} spike is not as large as expected from in vitro measurements.

There are several possible reasons for the lack of a Ca^{2+} spike in our experiments: 1) there might be a localized submembrane Ca^{2+} buffer of sufficiently high concentration and fast enough on-rate to attenuate significantly or eliminate the Ca^{2+} spike; 2) the on-rate for DPTA, which is unknown, may be fast enough to blunt or eliminate a Ca^{2+} spike; 3) the photolysis rate of DM-nitrophen in cytoplasm might be substantially slower than in vitro; 4) the three Ca^{2+} binding steps might have different kinetics and affinities, such that the Ca^{2+} spike loads only some Ca^{2+}-binding steps, but not all that are necessary to cause secretion. Without a direct measurement of the magnitude and time course of the submembrane Ca^{2+} spike, we cannot distinguish these possibilities.

Are there two populations of cells?

The responses of about half of the cells studied could be better approximated with a slower rate-limiting step ($\gamma = 100$ s^{-1}). Indeed, it is known that adrenal glands have cells that contain predominantly either adrenaline or noradrenaline, and our method of preparation of the cells can lead to a mixed population of cells. Further experiments are needed to clarify whether the different capacitance time courses are correlated to different cell types.

We have modeled a two-component rising time course by including two reserve pools in series. However, we could equally well have simulated the time course with two parallel release pathways or to two different types of vesicles, each with slightly different kinetics. Then, to explain the data, we would have to postulate that some cells have only the slower pathway and others have both. In this regard it is interesting to note that the maximum rate constants for the cells that have the slower, single-exponential response are around 30–60 s^{-1}, very similar to the maximum rates for melanotrophs, whereas fast class responses reach values up to 1000 s^{-1}.

Alternatively, one could imagine that cells have a regulatory mechanism that may alter the final step of secretion (rate γ in our Scheme 1) and that the percentage of vesicles falling into each component could be variable. This is indeed what is observed. The ratio of fast to slow amplitude is highly variable. Maybe cells differentiate in culture, gaining neuron-like characteristics of fast secretion.

REFERENCES

Armstrong, C. M. 1969. Inactivation of the potassium conductance and related phenomena caused by quaternary ammonium ion injected in squid axon. J. Gen. Physiol. 54:553–568.

Augustine, G. J., and E. Neher. 1992. Calcium requirements for secretion in bovine chromaffin cells. J. Physiol. 450:247–271.

Bazbek, A. D., and T. C. Südhof. 1994. A single C_2 domain from synaptotagmin I is sufficient for high affinity Ca^{2+}/phospholipid binding. J. Biol. Chem. 268:26386–26390.

Bittner, M. A., and R. W. Holz. 1992. Kinetic analysis of secretion from permeabilized adrenal chromaffin cells reveals distinct components. J. Biol. Chem. 267:16219–16225.

Bittner, G. D., and D. Kennedy. 1970. Quantitative aspects of transmitter release. J. Cell Biol. 47:585–592.

Brose, N., A. G. Petrenko, T. C. Südhof, and R. Jahn. 1992. Synaptotagmin: a calcium sensor on the synaptic vesicle surface. Science. 256:1021–1025.

Chow, R. H., and L. v. Rüden. 1994. Electrochemical detection of secretion from single cells. In Single-Channel Recording, 2nd ed, B. Sakmann, and E. Neher, editors. Plenum Press, New York.

Chow, R. H., L. von Rüden, and E. Neher. 1992. Delay in vesicle fusion revealed by electrochemical monitoring of single secretory events in adrenal chromaffin cells. Nature. 356:60–63.

Cohen, M. W., O. T. Jones, and K. J. Angelides. 1991. Distribution of Ca^{2+} channels on frog motor nerve terminals revealed by fluorescent ω-conotoxin. J. Neurosci. 11:1032–1039.

Fenwick, E., A. Marty, and E. Neher. 1982. Sodium and calcium channels in bovine chromaffin cells. *J. Physiol.* 331:599–635.

Glenny, B., M. A. Tack, and A. Powell. 1987. Calpactins: two distinct Ca-regulated phospholipid- and actin-binding proteins isolated from lung and placenta. *J. Cell Biol.* 104:503–511.

Grynkiewicz, G., M. Poeenie, and R. Y. Tsien. 1985. A new generation of Ca^{2+} indicators with greatly improved fluorescence properties. *J. Biol. Chem.* 260:3440–3450.

Hamill, O. P., A. Marty, E. Neher, B. Sakmann, and F. J. Sigworth. 1981. Improved patch-clamp techniques for high resolution current recordings from cells and cell-free membrane patches. *Pfluegers Arch. Eur. J. Physiol.* 391:85–100

Heinemann, C., L. von Rüden, R. H. Chow, and E. Neher. 1993. A two-step model of secretion control in neuroendocrine cells. *Pfluegers Arch. Eur. J. Physiol.* 424:105–112.

Horowitz, P., and W. Hill. 1989. The Art of Electronics, 2nd ed, Cambridge University Press, Cambridge. 58.

Jahn, R, and T. C. Südhof. 1994. Synaptic vesicles and exocytosis. *Annu. Rev. Neurosci.* 17:219–246.

Jahromi, S. S., and H. L. Atwood. 1974. Three-dimensional ultrastructure of the crayfish neuromuscular apparatus. *J. Cell Biol.* 63:599–613.

Kaplan, J. H., and G. C. R. Ellis-Davis. 1988. Photolabile chelators for rapid photolytic release of divalent cations. *Proc. Natl. Acad. Sci. USA* 85: 6571–6575.

♪ Kasai, H. 1993. Cytosolic Ca^{2+} gradients, Ca^{2+} binding proteins and synaptic plasticity. *Neurosci. Res.* 16:1–7.

Katz, B., and R. Miledi. 1965. The measurement of synaptic delay, and the time course of acetylcholine release at the neuromuscular junction. *J. Physiol.* 161:483–495.

Kawagoe, K. T., J. B. Zimmerman, and R. M. Wightman. 1993. Principles of voltammetry and microelectrode surface states. *J. Neurosci. Meth.* 48:225–240.

Konishi, M., S. Hollingworth, A. B. Harkins, and S. M. Baylor. 1991. Myoplasmic calcium transients in intact frog skeletal muscle fibers monitored with the fluorescent indicator furaptra. *J. Gen. Physiol.* 97:271–301.

Lindau, M., and E. Neher. 1988. Patch-clamp techniques for time-resolved capacitance measurements in single cells. *Pfluegers Arch. Eur. J. Physiol.* 411:137–146.

Neher, E., and A. Marty. 1982. Discrete changes of cell membrane capacitance observed under conditions of enhanced secretion in bovine chromaffin cells. *Proc. Natl. Acad. Sci. USA* 79:6712–6716.

Neher, E., and R. S. Zucker. 1993. Multiple calcium-dependent processes related to secretion in bovine chromaffin cells. *Neuron.* 10:21–30.

♪ Nowycky, M. C., and M. J. Pinter. 1993. Time course of calcium and calcium-bound buffers following calcium influx in a model cell. *Biophys. J.* 64:77–91.

Parnas, H., G. Hovav, and I. Parnas. 1989. The effect of Ca^{2+} diffusion on the time course of neurotransmitter release. *Biophys. J.* 55:859–874.

Robitaille, R., E. M. Adler, and M. P. Charlton. 1990. Strategic localization of calcium channels at transmitter release sites of frog neuromuscular synapses. *Neuron.* 5:773–779.

Thomas, P., A. K. Lee, J. G. Wong, and W. Almers. 1994. A triggered mechanism retrieves membrane in seconds after Ca^{2+}-stimulated exocytosis in single pituitary cells. *J. Cell Biol.* 124:667–675.

Thomas, P., J. G. Wong, and W. Almers. 1993a. Millisecond studies of secretion in single rat pituitary cells stimulated by flash photolysis of caged Ca^{2+}. *EMBO J.* 12:303–306.

Thomas, P., J. G. Wong, A. K. Lee, and W. Almers. 1993b. A low affinity Ca^{2+} receptor controls the final steps in peptide secretion from pituitary melanotrophs. *Neuron.* 11:93–104.

Trifaró, J. M., and M. L. Vitale. 1993. Cytoskeleton dynamics during neurotransmitter release. *TINS.* 16:466–472.

von Rüden, L., and E. Neher. 1993. A Ca-dependent early step in the release of catecholamines from adrenal chromaffin cells. *Science.* 262:1061–1065.

Wang, W., and C. E. Creutz. 1992. Regulation of chromaffin granule aggregation activity of annexin I by phosphorylation. *Biochem. J.* 31: 9934–9939.

◄ Yamada, W. M., and R. S. Zucker. 1992. Time course of transmitter release calculated from simulations of a calcium diffusion model. *Biophys. J.* 61:671–682.

◦ Zhou, Z., and E. Neher. 1993. Mobile and immobile calcium buffers in bovine adrenal chromaffin cells. *J. Physiol.* 469:245–273.

Zucker, R. S. 1973. Changes in the statistics of transmitter release during facilitation. *J. Physiol.* 229:787–810.

Zucker, R. S. 1992. Effects of photolabile Ca chelators on fluorescent Ca indicators. *Cell Calcium.* 13:29–40.

Zucker, R. S. 1993a. The Ca concentration clamp: spikes and reversible pulses using the photolabile chelator DM-nitrophen. *Cell Calcium.* 14: 87–100.

Zucker, R. S. 1993b. Calcium and transmitter release. *J. Physiol. (Paris).* 87:25–36.